Methods in Oceanography 17 (2016) 206–220

Contents lists available at ScienceDirect

Methods in Oceanography

journal homepage: www.elsevier.com/locate/mio

Full length article

Practical calibration of ship-mounted omni-directional fisheries sonars

Gavin J. Macaulay [a,*], Sindre Vatnehol [a], Ole Bernt Gammelsæter [b], Héctor Peña [a], Egil Ona [a]

[a] Institute of Marine Research, P.O. Box 1870 Nordnes, N-5817 Bergen, Norway
[b] Kongsberg Maritime AS, Strandpromenaden 50, 3191, Horten, Norway

HIGHLIGHTS

- Calibration is essential for quantitative use of fisheries sonar backscatter.
- A method for calibration of ship-mounted fisheries sonars is proposed.
- We measured and corrected for the effect of sonar configuration on the calibration.
- The accuracy and stability of sonar calibrations are measured.

ARTICLE INFO

Article history:
Received 12 July 2016
Received in revised form
27 September 2016
Accepted 11 October 2016

Keywords:
Omni-directional fisheries sonar
Calibration
Echo-integration

ABSTRACT

Conventional ship-mounted vertically-oriented echosounders are poor at detecting organisms that are close to the sea surface. In contrast, omni-directional sonars can ensonify these near-surface waters unavailable to hull-mounted echosounders. If calibrated, sonars can provide quantitative biomass estimates of pelagic aggregations. However, for sonars that have not been designed as scientific and research instruments, the quantification and verification of the system performance is of heightened importance, and should include how parameters such as the shape and gain of the beams vary with system and operational configurations. We present a practical methodology for absolute calibration of omni-directional sonars when conventionally mounted on a vessel, illustrate the achievable calibration accuracies and precision, and document their variability over time and for a range of operating parameters. This work forms an essential prerequisite to the use of such sonars for quantitative measurement of backscatter, such

* Corresponding author.
E-mail address: gavin.macaulay@imr.no (G.J. Macaulay).

http://dx.doi.org/10.1016/j.mio.2016.10.001

as for echo-integration surveys and individual school density and biomass estimation.

1. Introduction

Downward-looking, narrow-beam echosounders are commonly used for quantitative acoustic surveys of fish populations, being relatively simple to operate with well-developed analysis procedures for producing biomass estimates (Simmonds and MacLennan, 2005). However, they are not the ideal tool for detecting organisms that are close to the sea surface because most ship-based installations have the transducers mounted some metres below the surface to avoid the deleterious effects of air bubbles (Dalen and Løvik, 1981). In conjunction with the transducer near-field, transducer ringing, and the increasingly popular use of lowerable keel-mounted transducers, it is common that no echoes can be quantitatively measured in the upper 5–15 m. Also, at typical marine survey speeds (approx. 5 m/s), the probability of detecting small near-surface aggregations is low.

Omni-directional sonars are commonly used in pelagic fisheries, where they aid in finding and assessing fish aggregations, and monitoring the catch process (Ben-Yami, 1994). These sonars form acoustic beams from an array of transducer elements in a range of directions (Sherman and Butler, 2007). The most common arrangement is to form many narrow beams with oval cross-section that are emitted radially in all directions from the transducer, with a configurable tilt angle relative to horizontal, commonly called the horizontal mode. Some systems also form a vertical fan of beams with a configurable azimuth direction, commonly called the vertical mode.

Omni-directional sonars can provide information on schools metrics, speed, and behaviour (Misund, 1990; Misund et al., 1996; Peraltilla and Bertrand, 2014; Stockwell et al., 2013; Trygonis et al., 2016), but in most instances the backscatter amplitude information has not been used in a quantitative manner analogous to the echo-integration method commonly used with narrow-beam echosounders. Lack of access to calibrated quantitative backscatter has restricted most work to the analysis of the sonar's presentation display (Brehmer et al., 2006; Brehmer and Gerlotto, 2001; Trygonis et al., 2009), with compromises in dynamic range, linearity, and backscatter measurement accuracy.

While omni-directional sonars are able to better sample near-surface waters due to the horizontally-oriented beams, and can provide quantitative estimates of pelagic biomass (Brehmer et al., 2006; Misund, 1993, 1990; Smith, 1970), they introduce other complexities. Ensonifying organisms at variable side-aspect angles increases the variation in acoustic reflectivity (Cutter and Demer, 2007; Holmin et al., 2012; Tang et al., 2009), requires a more complicated echo-integration method (Nishimori et al., 2009), and acoustic ray bending (Brehmer et al., 2006; Lichte, 1919) complicates the survey sampling strategy.

Quantitative use of sonar backscatter data requires a known and stable relationship between acoustic and recorded amplitude over the range of sonar operating modes that are used in a study or survey — that is, the sonar should be calibrated. For systems that have not been intended for use as scientific instruments, the quantification and verification of system performance is of heightened importance. This should include knowledge on how parameters such as the shape and gain of the beams vary with system and operational configurations. Most omni-directional sonars provide the ability to set the acoustic frequency, pulse duration, pulse form, beamwidth, and tilt angle. For the sonars considered in this paper the total number of unique combinations of these settings exceeds 98 000. When combined with the 64 beams available in these sonars, there are more than six million potential combinations and is overwhelmingly impractical to calibrate all of them. A better approach is to understand the independent effect of each setting, so that relative adjustments can be applied to a small number of calibrations. Variation in beam characteristics and the associated calibration can be predicted via theoretical considerations of the underlying sonar transmit and receive operations, but the actual performance of individual sonars can vary significantly from the theoretical (Cochrane et al., 2003).

Calibration can be achieved via several methods, such as reciprocity or a calibrated hydrophone (Foote et al., 1987), but the most common method uses metallic spheres of known reflectivity (Foote and MacLennan, 1984). Sphere-based calibration has been demonstrated for multi-beam sonars, which produce a linear fan of beams, in controlled conditions such as tanks or enclosed environments (Cochrane et al., 2003; Foote et al., 2005; Lanzoni and Weber, 2011; Melvin et al., 2003; Perrot et al., 2014) and for omni-directional sonars, but without thorough quantification of the beam parameters (Bernasconi, 2012; Geoffroy et al., 2015; Nishimori et al., 2009). More advanced scientific sonars, such as the Simrad MS70, are readily calibrated by the sphere method (Ona et al., 2009).

The largest and most readily available pool of omni-directional sonars of relevance to fisheries research are on pelagic fishing and research vessels. The sonar transducer is on a retractable pole insert into the hull. As a consequence, the onboard computing, electrical, and mechanical systems that comprise the sonar are bulky and difficult to remove for separate calibration in a controlled environment. However, time-efficient calibration of ship-mounted omni-directional sonars in uncontrolled environments is now practical via a purpose-built calibration sphere positioning apparatus (Vatnehol et al., 2015), which can be used to measure system gain and the beam parameters required for measurement of volume backscatter. The ability to digitally record and analyse beam-formed sample data is also necessary. Together, these developments facilitate the calibration of ship-mounted omni-directional sonars.

This paper presents a practical methodology for absolute calibration of ship-mounted omni-directional sonars and thereby demonstrates the application of a solution (Vatnehol et al., 2015) to the previously identified problem of calibrating multibeam sonars when affixed to the hull of a ship (Foote et al., 2005). This methodology is applied to the Simrad SX90 and SU90 sonars, illustrates the achievable calibration accuracies and precision, and quantifies their stability over time and for a range of operating parameters. This work forms a prerequisite to the routine use of such sonars for quantitative volume backscatter measurement, as is required for echo-integration surveys and individual school density and biomass estimation.

2. Methods

2.1. Theory

The Simrad SX90 omni-directional sonar operates at a user-configurable frequency between 20 and 30 kHz inclusive. In horizontal mode it utilises its 256 element vertically-oriented cylindrical transducer to form 64 receive beams with selectable declination relative to horizontal. The transducer is used for both transmission and reception — the transmitted beam is omni-directional in the horizontal plane, but covers a narrow angle in the vertical plane. Each SX90 two-way beam has a nominal vertical cross-section that varies from 7.7° (at 20 kHz) to 5.1° (at 30 kHz) and a horizontal cross-section of between 13.0° (20 kHz) and 8.6° (30 kHz). The Simrad SU90 sonar is functionally the same as the SX90 except that the cylindrical transducer array is taller, comprising 384 elements and produces vertically narrower beams than the SX90 sonar (5.4° to 3.6°). Both systems can transmit at a single frequency (labelled here as CW) or with a hyperbolic frequency modulated (FM) signal with 500 Hz bandwidth, at various pulse lengths. The vertical beamwidth can also be set to one of three options (narrow, normal, or wide). Echoes are processed with a matched filter derived from the transmitted signal. The sonar records beamformed data in the form of complex demodulated, pulse-compressed estimates of the power received by each beam at a decimated sample rate determined by the sonar configuration (typically 4 kHz). For the horizontal beam mode, this is converted into backscattered target strength (TS) via a power-budget formulation (Lunde and Korneliussen, 2016) provided by the manufacturer:

$$TS = 10\log_{10}(P_r) + 40\log_{10}(r) + 2\alpha r - 10\log_{10}\left(\frac{P_t\lambda^2}{16\pi^2}\right) - G(\theta,\phi) - 40\log_{10}(\cos\gamma), \quad (1)$$

where P_r is linearly proportional to the received power (W), r the range between the transducer and target (m), α the absorption coefficient of sound in water (dB m^{-1}), P_t the transmit power (W), λ the

acoustic wavelength (m), $G(\theta, \phi)$ the transducer gain in the direction of the target (dB), and γ the beam tilt angle (degrees from horizontal). The $40 \log_{10}(\cos \gamma)$ term compensates for the loss in beam power as the tilt deviates from perpendicular to the transducer. The volume backscatter strength (S_v, MacLennan et al., 2002) is derived from a similar equation:

$$S_v = 10 \log_{10}(P_r) + 20 \log_{10}(r) + 2\alpha r - 10 \log_{10}\left(\frac{P_t \lambda^2 c \psi \tau_e}{32\pi^2}\right) - G_0 - 40 \log_{10}(\cos \gamma) \quad (2)$$

where c is the acoustic sound speed (m/s), and ψ the equivalent beam angle (sr), τ_e the effective pulse duration (s), and G_0 the on-axis transducer gain (dB), equivalent to $G(0, 0)$. The effective pulse duration is estimated from the calibration sphere echo using:

$$\tau_e = \frac{\int P_r dt}{P_{r,m}},$$

where $P_{r,m}$ is the maximum of P_r. In practice, τ_e is calculated via summation of the discrete samples from the sphere echo. Note that the use of τ_e in Eq. (2) has the same effect as the combination of nominal pulse length and the $S_{a,corr}$ parameter that is used with other Simrad sonars and echosounder S_v equations (Demer et al., 2015; Ona et al., 2009).

The location of the calibration sphere in the acoustic beam was estimated using a calibration rig that gave the precise three-dimensional location of the sphere relative to a reference point (Vatnehol et al., 2015). An empirical beam pattern was defined as (Jech et al., 2005):

$$\begin{aligned} b^2 &= 10 \log_{10}(2) \left(\alpha^2 + \beta^2 - 0.18\alpha^2\beta^2\right), \\ \alpha &= \frac{2(\theta + \theta_o)}{\theta_{BW}}, \\ \beta &= \frac{2(\phi + \phi_o)}{\phi_{BW}}, \end{aligned} \quad (3)$$

where b^2 is the two-way beam pattern (and hence $G(\theta, \phi) = G_0 + b^2$), α and β dimensionless terms that serve to clarify the form of b^2, θ the vertical beam coordinate (°), θ_o the vertical beam offset (°), and θ_{BW} the vertical half-power two-way beamwidth (°). Similar variables for the horizontal beam coordinate are given by the ϕ variables. As most of the transmitted energy from each beam is in the main lobe (Reynisson, 1998), the equivalent beam angle was estimated from the integral of the beam pattern function (Eq. (3)) fitted to the sphere echo data:

$$\psi = \int_{4\pi} b^2 d\Omega, \quad (4)$$

where b^2 is the two-way beam pattern obtained from the sphere echo measurements, normalised to unity on the acoustic axis of the transducer, and $d\Omega$ the solid angle. In practice the integration was limited to twice the estimated half-power beamwidth, corresponding approximately to the −12 dB points in the two-way directivity response of each beam.

The echo range in the sonar data files is not given directly, but must be derived from the sound speed in water, the time since sampling began, and any processing delays. Not all of the processing delays are necessarily compensated for by the sonar and the conversion between sample and range was assumed to be:

$$r = \frac{c \cdot dt}{2} i - r_o, \quad (5)$$

where dt is the time interval between samples (s), i the sample number (from zero to one less than the number of samples) and r_o an empirically derived offset that is independent of the sonar operating parameters. This offset is due to an approximately 4 ms delay in the signal processing operations of the SX90 and SU90 sonars that is not compensated for in the recorded data. To verify this, the true distance between the sonar transducer and the sphere was measured. The locations of the various pivot points

of the 'multi-beam' calibration rig boom (Vatnehol et al., 2015) were measured relative to a common reference point on the vessel foredeck. The position of the pivot point relative to the sonar transducer was then calculated using dimensioned ship drawings. Given the azimuth angle of a particular sonar beam, the length of the boom, and the beam tilt angle, the distance between the sonar transducer and the sphere was calculated. The rig was adjusted so that the boom was horizontal with the sphere hanging directly below the boom end. Motion of the sphere due to vessel or water movements was small. The true sphere range was estimated for multiple sphere ranges, sonar beams, and three pivot point locations. The mean difference between the true and sonar ranges was used as an estimate of r_0 in Eq. (5).

The calibration methodology used in this study was directed by earlier work on protocols for calibrating multibeam sonars (Cochrane et al., 2003; Foote et al., 2005; Ona et al., 2009), modified to suit the particular characteristics of omni-directional sonars and their physical installation onboard vessels.

2.2. Calibration procedure

Calibrations were carried out using SX90 sonars on three ships (RV *G.O. Sars*, FV *Artus*, and FV *Brennholm*) and SU90 sonars on two ships (FV *Kings Bay* and FV *Eros*) when moored or anchored in fjords on Norway's west coast. The water depth below the vessels was always greater than 30 m.

Two different calibration rigs were used to move the sphere within the sonar beams (Vatnehol et al., 2015). The 'precision' rig provided accurate relative horizontal and vertical sphere position and was used to measure the vertical and horizontal beam shape. The 'multi-beam' rig provided only accurate relative vertical sphere position, but was easier and faster to use, enabling the coverage of more beams. For this rig the sphere was instead centred horizontally by moving the sphere so that the amplitude observed on the two surrounding beams was equal (which occurs when the sphere is in the centre of the central beam). This rig was used for all other calibration activities.

For each calibration the appropriate rig was affixed to the ship deck in the vicinity of the sonar transducer and the rig extended out over the side of the ship (Fig. 1). A sphere was suspended from the end of the boom and lowered until it was visible in the sonar display. The vertical position of the sphere relative to the beam centre was measured by the calibration rig and the angular position of the sphere, relative to the beam direction, was obtained by numerically solving for ω in:

$$\cos(\varepsilon + \omega)\tan\varepsilon + \frac{d}{r} = \sin(\varepsilon + \omega)\,, \tag{6}$$

where ε is the beam angle below horizontal, ω the within-beam angle of the sphere, d the vertical distance from beam centre, and r the distance from the transducer to the sphere (Fig. 1). When the 'precision' rig was used, the horizontal angle of the sphere relative to the beam direction was calculated by taking the inverse sine of the ratio of the horizontal sphere offset from beam centre and the range to the sphere. The amplitude of the sphere echo was calculated from the beam-formed data via Eq. (1).

The sonar performance was measured using sonars on the five ships (Table 1):

- *On-axis gain* was estimated for multiple beams by centring the sphere in the selected beam and recording backscatter amplitude from at least 100 pings. The sphere was then moved to an adjacent beam and the procedure repeated. This process continued for as many beams as possible, with changes to the rig's location as required.
- The *vertical and horizontal beamwidth* was estimated for selected beams by moving the sphere vertically and horizontally within the selected beams. The 'precision' rig was used.
- The *gain and vertical beamwidth* was estimated for selected beams by placing the sphere in the centre of the beam. The sphere was then moved vertically to map the vertical beam shape. Several beams were mapped while systematically varying the acoustic frequency, formed beamwidth, and beam tilt angle.
- The *effect of pulse parameters* on transducer gain was measured by keeping the sphere stationary in one beam while the frequency, pulse length and pulse type were systematically varied.

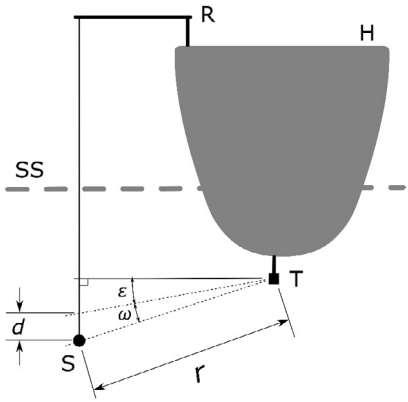

Fig. 1. Schematic of the calibration setup showing the vessel hull (H), calibration rig (R), sea surface (SS), calibration sphere (S), and sonar transducer (T). The labelled dimensions are used in Eq. (6).

Table 1
The vessels and sonars used for the various calibration objectives.

Calibration objective	Vessel(s)	Date	Sonar
On-axis gain	RV *G.O. Sars*. FV *Artus*	November 2013	SX90
Vertical and horizontal beamwidth	FV *Artus*	March 2013	SX90
Effect of frequency, formed beamwidth and tilt on gain and vertical beamwidth	FV *Eros*	October 2015	SU90
Effect of pulse parameters on gain	FV *Brennholm*	October 2012	SX90
Range	FV *Kings Bay*	October 2014	SU90
Medium-term variation of gain	RV *G.O. Sars*	October 2015	SU90
Long-term variation of gain	FV *Kings Bay*	October 2014, May 2016	SU90

- The *range from the transducer* to the sphere was physically measured with the sphere at nine different distances.
- The *medium-term variability* of gain estimates was estimated by placing the sphere in the centre of one beam and sphere backscatter amplitude recorded over a period of approximately 25 min.
- The *long-term stability* of gain estimates was illustrated by comparing gain estimates from calibrations of the same ship and sonar carried out at different times.

The SX90 and SU90 offer user-configurable filters which modify the backscatter data prior to presentation to the sonar operator. One of these (the 'noise filter') is applied prior to recording of the backscatter data and this filter was turned off during the calibrations.

A conductivity-temperature-depth (CTD) cast was carried out during each calibration and used to estimate acoustic absorption (Francois and Garrison, 1982), sound speed (Chen and Millero, 1977), and density (Fofonoff and Millard, 1983) profiles over the depth range between the sonar transducer and calibration sphere. The harmonic mean of the sound speed and arithmetic mean of the absorption estimates were used in subsequent processing. No CTD was taken for the FV *Brennholm* calibration and nominal values were used (a temperature of 10 ° C and salinity of 35 PSU).

Two tungsten carbide spheres (with 6% cobalt binder) were used for the calibrations. The diameter was 75 mm for the FV *Brennholm* calibration and 64 mm for the other calibrations. These spheres were chosen for their strong and slowly varying reflectivity in the sonar operating range (20 to 30 kHz). They are also heavy (3.3 and 2 kg) and are less affected by water movements than lighter spheres. The expected backscatter strength was estimated from theory (Hickling, 1962; MacLennan, 1981) for the environmental conditions experienced during the calibrations.

The sonar calibrations on all vessels except for FV *Brennholm* and FV *Kings Bay* in 2016 used a 4 kW CW transmit pulse of 2 ms duration. The acoustic frequency was varied as required. The calibration on

FV *Brennholm* used pulse durations of 1, 2, and 6 ms with a CW signal and pulse duration of 2, 4, and 6 ms with an FM signal. All six settings were used at operating frequencies of 20, 23, 26, and 28 kHz. The 2016 calibration on FV *Kings Bay* used an FM signal of 4 ms duration.

The distance between the sonar transducer and calibration sphere was always greater than twice the estimated near-field range, obtained from the equation for the near-field range of a rectangular planar transducer (Medwin and Clay, 1998):

$$r_{nf} = \frac{A}{\lambda}, \tag{7}$$

where r_{nf} is the near field range (m), A is conservatively taken as the square of the maximum transducer dimension (m^2), and λ the acoustic wavelength (m). The SX90 transducer array has a height of approximately 0.33 m, the SU90 a height of 0.50 m, and both have a diameter of approximately 0.37 m. The longest near-field range is then 5.1 m (SU90 at 30 kHz).

2.3. Analysis

The on-axis transducer gain (G_0) for each beam was estimated using purpose-built software that read the sonar data files and produced a sonar image where a beam of interest could be selected, and range and time period limits applied. Sphere echoes were discarded if the 10-ping running mean of the sphere amplitude in the two surrounding beams differed by more than 3 dB, as were datasets where the standard deviation of the range to the sphere varied by more than 0.05 m. The maximum amplitude of the sphere echo was then estimated for the selected beam, range, and time periods. The maximum echo amplitude was obtained from the peak of a quadratic function fitted to the three sample values that defined the peak and the transducer gain calculated using Eq. (1). At least 100 echoes from the sphere were collected and the linear mean and root-mean-square (RMS) of the sphere echoes calculated. The beam mapping data were processed in a similar way, but with the addition of the sphere angle relative to on-axis. The half-power, two-way vertical and horizontal beamwidths were estimated by fitting Eq. (3) to the sphere backscatter and position data using non-linear least squares minimisation. The RMS values were calculated from the dB difference between the fitted equation and the individual sphere target strengths measurements used in the fitting process.

The variation in gain due to both frequency and pulse length was observed to have asymptotic behaviours and an empirical relationship was derived from these data using least-squares minimisation.

We assumed that the theoretical beam gain was identical for all beams and that any observed variation was due to factors such as changing propagation conditions, unaccounted for sphere motion within the beam, and variation in sonar transducer and transceiver performance. Under this assumption we calculated a single value for G_0 from the measured beam gains by removing beams with an RMS value greater than 1.5 dB and taking the mean in linear space of the remaining G_0 values.

3. Results

On-axis gain and medium-term variability: The estimated on-axis gain for individual beams in an individual sonar had a typical RMS of 0.5 dB, with some exceeding 1.0 dB (Fig. 2(a), (d)). Overall, the mean gain variation was $\pm$0.7 dB for RV *G.O. Sars* and $\pm$0.8 dB for FV *Artus*. The variability in gain for a single beam over an extended period was approximately $\pm$1 dB (Fig. 3).

Vertical and horizontal beamwidth: The empirical beam shape was typically a good representation of the measured beam shape (Fig. 4) and the resulting estimates of beamwidth have a high confidence (Table 2).

Gain and vertical beamwidth: The trends in beamwidth with changing frequency, requested beamwidth, and beam tilt were as expected (beamwidth decreases as frequency increases, beamwidth increases with increasing requested beamwidth, and beamwidth is constant with beam tilt, Fig. 5). The

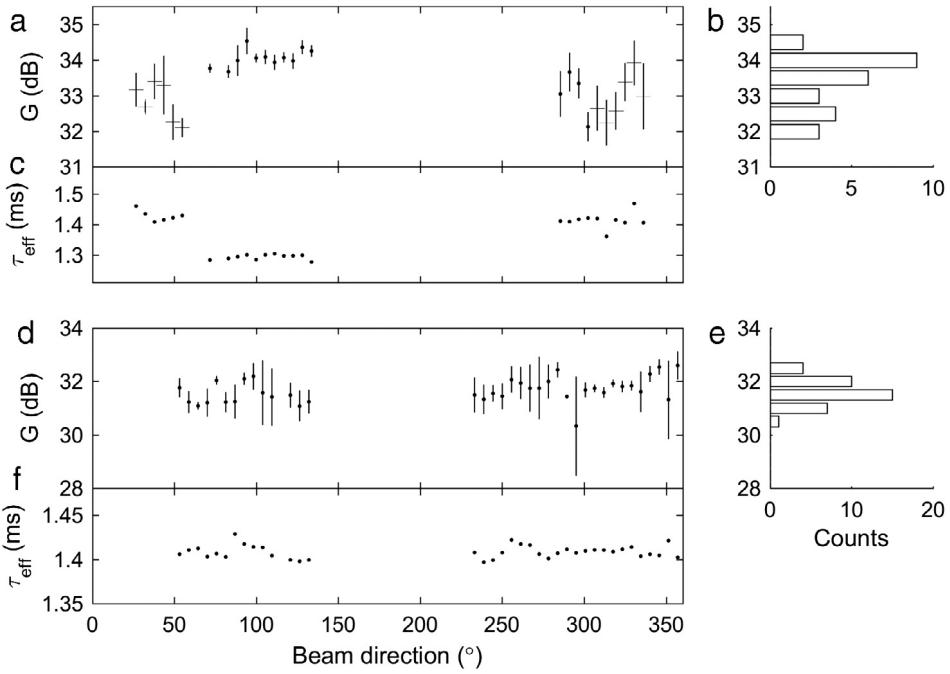

Fig. 2. On-axis gain estimates, distribution, and effective pulse duration for the November 2013 calibrations of selected beams on the SX90 sonars of RV *G.O. Sars* (a, b, c) and FV *Artus* (d, e, f). The G.O. Sars estimates are for a beam tilt of -10° $(\cdot)$ and -25° $(+)$, a transmit frequency of 26 kHz, using a CW pulse of 2 ms nominal duration. The FV *Artus* estimates are for a beam tilt of -3°, transmit frequency of 30 kHz using a CW pulse of 2 ms nominal duration. The vertical lines show the root-mean-square (RMS) of the gain estimates about the mean ($\pm$RMS). A beam direction of 0° indicates the vessel's bow, increasing clockwise.

trends in transducer gain were also as expected (gain increases as frequency increases, gain decreases as beamwidth increases, and gain remains constant with beam tilt, Fig. 5).

Effect of pulse parameters: The gain increased with longer pulse durations and higher frequencies with an asymptotic form (Fig. 6). The effect of pulse duration on gain was independent of the effect of frequency on gain. The changes in gain were not affected by the pulse type (CW or FM). These systematic changes in beam gain were fitted with a correction function:

$$G_c\,(f,\tau) = \frac{3.69\times 10^3}{f} - \frac{53.9\times 10^6}{f^2} - \frac{6.49\times 10^{-3}}{\tau} - 43.2, \tag{8}$$

where $G_c\,(f,\tau)$ is the gain correction (dB) relative to that obtained for a transmit pulse of length 1 ms and frequency 20 kHz, where f is frequency (Hz) and τ the nominal pulse length (s). The RMS of the deviation of the measured gains from Eq. (8) was 0.58 dB (comprised of 0.38 dB for the frequency component and 0.36 dB for the pulse duration component). Eq. (8) has only been validated for $20 \le f \le 30$ kHz and $1 \le \tau \le 8$ ms. The correct gain for survey settings is then obtained by applying the difference in gain corrections between the calibration settings and survey settings thus:

$$G_{0,survey} = G_{0,cal} + \left[G_{c,survey} - G_{c,cal}\right], \tag{9}$$

where the *survey* and *cal* suffices indicate the applicability of the parameters. Note that Eq. (8) incorporates the effect on G_0 of any change in the pulse length between calibration and survey settings. This means that the pulse length used during the calibration should be applied in Eq. (2) regardless of the actual pulse length.

Range: The mean difference between the sonar estimated sphere range and the measured range was 2.99 m (Fig. 7), closely agreeing with the manufacturer's 4 ms estimate of uncorrected processing delay (equivalent to 2.9898 m at the 1494.8 m/s sound speed measured during the experiment).

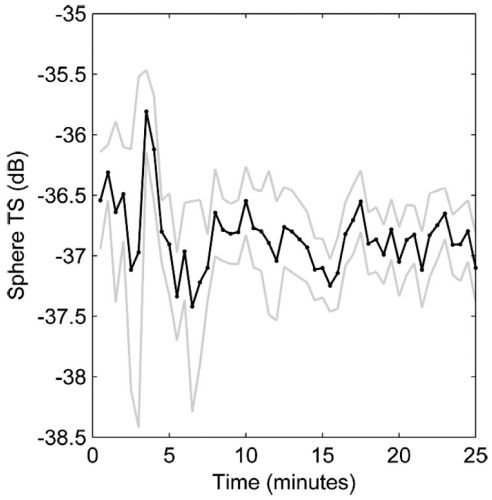

Fig. 3. Variation in sphere target strength with time. Mean TS over the preceding 60 pings (approximately 30 s) (black line) and the standard deviation of the preceding 60 pings (grey lines).

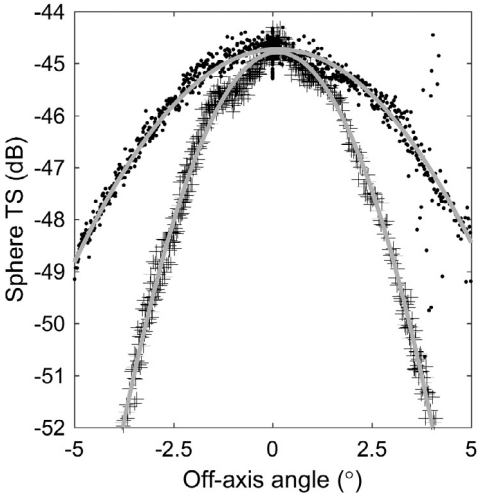

Fig. 4. Sphere target strength measurements along the vertical (plus symbols) and horizontal (dots) beam axes and fitted beam pattern relationship from the SX90 on FV *Artus* (March 2013 calibration, beam 49, −5° beam tilt, 30 kHz transmit frequency with a CW pulse 1 ms in duration).

Long-term variation of gain: The average G_0 from the 2016 calibration of nine beams on the SU90 on FV *Kings Bay* was 38.1 dB. The 2014 calibration of a similar set of nine beams was 36.5 dB, but after applying Eq. (9) to compensate for the difference in pulse lengths used, the G_0 value was estimated to be 38.1 dB, the same as for 2016.

4. Discussion

The use of omni-directional sonars in a quantitative acoustic survey requires adequate calibrations over the range of sonar settings that might be used during the survey, or an understanding of the effect of sonar settings on the calibration. Our experience is that there are five settings that are

Table 2
Beamwidth estimates (half-power, two-way), variability (RMS) and equivalent beam angles (ψ) for selected beams of the SX90 sonar on FV *Artus*. Beam tilt was 5°, frequency 30 kHz, and beam mode set to 'normal'.

Beam	Vertical beamwidth (°)	Horizontal beamwidth (°)	RMS of fit (dB)	ψ (sr)	Manufacturer provided ψ (sr)
31	5.3	9.0	0.3	0.0169	0.0162
49	5.0	8.9	0.2	0.0157	0.0162
60	5.0	8.9	0.3	0.0158	0.0162

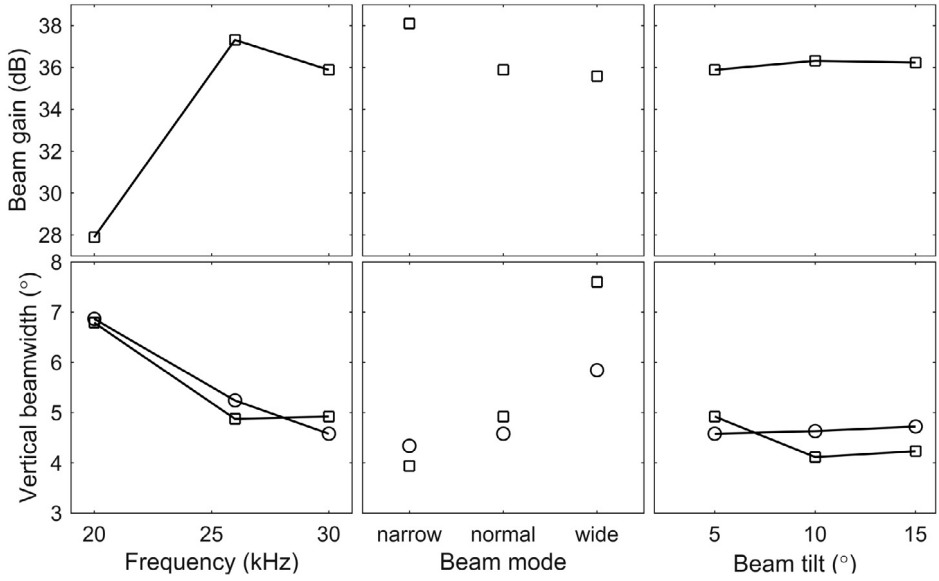

Fig. 5. Changes in beam gain (upper panels) and half-power two-way vertical beamwidth (lower panels) as a result of changes in sonar parameters for an SU90 beam on FV *Eros* (squares) and as derived from the sonar-provided one-way beamwidths (circles). When not varied, the beam mode was set to normal, frequency to 30 kHz, and beam tilt to 5°.

typically changed (Table 3), but with some planning this can be reduced to just one, the horizontal beam tilt angle. However, to maintain consistent observation ranges and depth during a survey the tilt angle should be constant, implying that the calibration configuration can be the same as the survey configuration. However, this is not always practical. For example, the best beam tilt angle for the calibration is determined by the local bathymetry, proximity of underwater structures, and the transducer to sphere range. This may not coincide with the desired survey tilt angle. Also, the SX90 and SU90 transmitted pulse length is set according to the maximum display range (longer display ranges result in longer transmit pulse durations). Furthermore, a fast ping rate is desirable during calibration as it improves responsiveness when moving the sphere and reduces the calibration duration. Hence the operating range is best kept short, while for surveys the operating range is typically larger. Even when using just one sonar setup for a survey it is therefore still necessary to quantify how the sonar performance varies with some of the sonar settings. This is in contrast to conventional single-beam scientific echosounders, where it is feasible and normal to calibrate the system using the same settings as used during the survey. In addition, any processing filters that are applied before data are recorded must be evaluated and either configured so that their effects are constant between calibration and survey settings, or turned off.

The estimated beam gains had a rather high RMS (typically $\pm$0.5 dB) compared to the $\pm$0.1 dB RMS that is routinely achieved with echosounders (Knudsen, 2009), but is still of sufficient accuracy for quantitative use. The use of Eq. (9) will increase the beam gain uncertainty — summation of errors in quadrature indicates an RMS gain uncertainty of $\pm$0.77 dB, compared to the $\pm$0.5 dB when not using

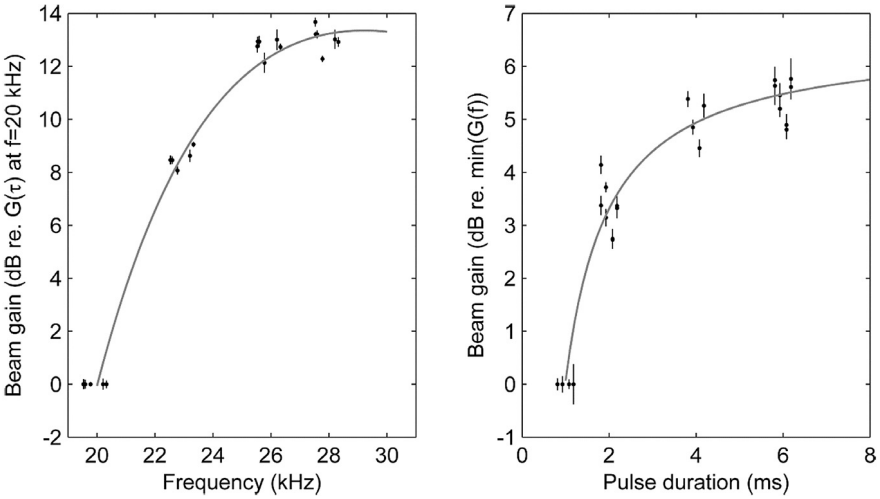

Fig. 6. Relative changes in the beam gain with the changes in the pulse frequency (left panel) and with changes in the pulse duration (right panel). Dots indicate measured beam gain from the SX90 on FV *Brennholm*, and the line indicates the asymptotic regression ($r^2 = 0.995$, left panel; 0.964, right panel). Jitter has been added to the x-axis values to more clearly separate the data points. The root-mean-square (RMS) of the sphere echoes about the mean value is indicated by the vertical lines (±RMS).

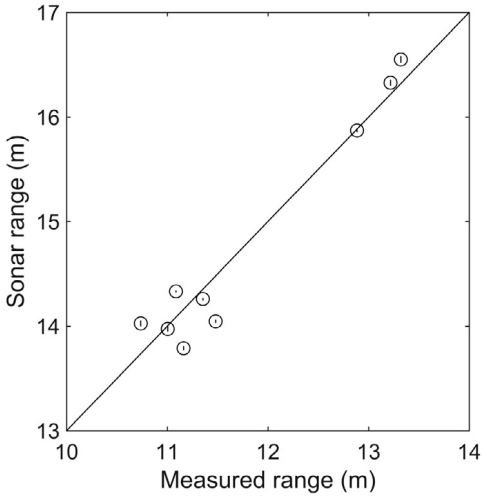

Fig. 7. Comparison of sphere range estimated by the sonar and physically measured sphere range. The root-mean-square (RMS) of the sonar range estimates is indicated by the vertical lines (±RMS). The solid line is the sonar range correction model, Eq. (5), fitted to these data. The mean difference in range estimates is 2.99 m.

Table 3
The influence of commonly varied SX90 and SU90 sonar settings on system configuration.

Sonar setting	Affects
Frequency	Beam shape (G_0, ψ)
Beamwidth	Beam shape (G_0, ψ)
Beam tilt	Beam shape (G_0, ψ)
Display range	Pulse length (G_0)
Pulse type	Pulse length (G_0)

Eq. (9). It is thus preferable to perform calibrations at the survey frequency and pulse duration. If this is not possible, a calibration performed at the survey frequency but different pulse duration (±0.62 dB) or vice-versa is preferred (±0.63 dB). The medium-term duration calibration (Fig. 3) indicates that this variability is dominated by either changing propagation conditions or variation in sonar performance. We postulate three reasons for this, (1) the sonar was not designed for stable quantitative scientific use and may not have high measurement stability, (2) variation in the propagation conditions between the sonar and the sphere may cause ray bending and associated changes in the received acoustic wave from the sphere, and (3) there is the potential for acoustic interference caused by multipath propagation, either via the sea surface, the seabed, or the ship's hull. All of our calibrations were conducted in sheltered fjords, where freshwater runoff and lack of strong winds can cause significant stratification with the potential for short-duration variations (Skarthhamar and Svendsen, 2010). All sound speed profiles taken during the calibrations showed some degree of stratification between the transducer and sphere depths and we anticipate that stratification, and short-term variation of, is the dominant cause of the observed calibration variability. Calibrating in an area with well-mixed near-surface waters is hence recommended.

An echosounder or sonar calibration has two aims: to provide the conversion factor between the system response and physically realisable measurements, and to ensure that the system is working correctly. Ideally, one would calibrate all beams to achieve both of these aims, but this is a time-consuming exercise and is difficult for the aft-pointing beams. However, for the SX90 sonar, a single beam is formed from a 12 by 8 array of transducer elements (Blomberg et al., 2012), being 37.5% of elements in the transducer. Calibration of three beams spaced 90 degrees apart from each other will utilise 87.5% of the elements and serve to check the correct functioning of that percentage of the transducer and transceiver elements and processing channels. Similarly, since adjacent sonar beams in the SX90 are formed from an almost identical set of transducer elements we hypothesise that the gain of an individual beam is strongly correlated with the gains of the adjacent beams. This implies that it is not necessary to calibrate adjacent beams because they will have substantially the same performance. However, the results obtained from RV *G.O. Sars* and FV *Artus* show an adjacent beam-to-beam gain difference of up to 1.3 dB (Fig. 2), which we attribute mainly to variability in the calibration process and environmental variability, and not beam performance. This can be caused by fluctuations in medium sound speed, multipath echoes via the sea surface, ship hull, anchor chain, and wharf piles, if present, and interference by backscatter from organisms in the water. With sufficient measurements, the mean is considered to be representative of the true value. In comparison, a tank-based calibration of a 22.5 kHz omni-directional sonar achieved a between-beam gain change of up to 1.5 dB (Nishimori et al., 2009), while a ship-based calibration of a 110 kHz omni-directional sonar found the between-beam received echo levels to vary by up to 5 dB (eight beams covering a 90° sector, (Bernasconi, 2012)). To obtain a robust calibration we recommend measuring the gain from three well-separated beam directions with the aim of exercising completely different sets of transducer elements. Due to the variability in adjacent beam gains (Fig. 2), we also recommend calibrating three or more adjacent beams to ensure that any single outlying beam calibration is identified and removed if necessary. An average of these beam gains is then applied to all beams of the sonar.

The SX90 and SU90 sonars can be taken as calibrated when all of the parameters in Eqs. (1), (2) and (5) have been estimated for the set of operating modes that will be used during quantitative surveys. Variations in transducer gain were observed due to changes in frequency and pulse length, despite these terms being in Eqs. (1) and (2). This emphasises the need to independently verify the calibration and effect of system parameters. This has been done for the SX90 and SU90 sonars and permits the calculation of a calibration for any frequency and pulse length combination via Eqs. (8) and (9). This has been demonstrated using two calibrations from the same ship and sonar, two years apart, but with different pulse lengths. The same gain value was obtained, also indicating that the sonar performance had remained constant over that period.

The range provided by the sonar was not an accurate estimate of the true range, being 2.99 m too large. Using the correct range is particularly important when calibrating at short ranges because the $\log_{10}(r)$ term in Eqs. (1) and (2) changes rapidly, leading to an incorrect gain estimate.

The work presented here does not account for any changes in beam shape and gain due to the automatic stabilisation of beam tilt performed by the sonar (in response to pitch and roll of the vessel).

The beam forming should have minimal effect on the beam characteristics, but the efficacy of this has not been confirmed. This could be tested by conducting a beam calibration while the attitude of the ship was systematically changed (or more simply by sending simulated motion-reference data to the sonar).

When conducting a calibration with the ship anchored, the anchor chain caused strong interfering echoes in up to four beams at a similar range as the calibration sphere and prevented calibration of those beams due to echo interference. When moored, wharf piles caused a similar problem. During surveys fish are mostly observed to the front and side of the vessel and the vessel propellers and wake create bubble clouds that generate strong backscatter in the aftward beams, hence the calibration of these beams was not prioritised. Our calibration rig could not place the sphere in the aftward beams but it would be possible to do so using a two-line suspension apparatus similar to the three-line systems used to calibrate echosounders on vessel hulls (Demer et al., 2015).

An accurate equivalent beam angle (ψ) value is important when calculating S_v. The 'multi-beam' calibration rig is unable to conveniently provide the beam opening angles that are required to calculate ψ and as per the conventional practise in echosounder surveys, the manufacturer-supplied value has been used. Supporting this, the measured ψ for the SX90 sonar agrees well with the manufacturer-supplied value (Table 2) and gives confidence that the lack of empirical ψ measurements will not lead to large errors in S_v for the sonars studied in this paper. Alternatively, the 'multi-beam' calibration rig could be modified to measure the rotation angle of the pole, the position of the pole's centre of rotation relative to the sonar measured, and the horizontal position of the sphere calculated. This would enable estimation of ψ. The split-beam method (Burdic, 1991; Demer et al., 1999) can be used to estimate the position of the calibration sphere in the beam. This would speed up the calibration process and allow for full mapping of the beam shape, but would not however provide an estimate of ψ.

This paper has considered only on the horizontal mode beams. Calibration of the vertical mode beams would proceed in a similar manner and similar results and conclusions would be expected.

While this work utilised omni-directional sonars from a single manufacturer, the general method, analysis procedures, and experiences are applicable to all omni-directional sonars. Of particular note is the need to pay close attention to all sonar settings that could affect the beam parameters, and to develop correction methods for these.

Confidence in the accuracy of the quantitative output from an omni-directional sonar provides a firm basis for addressing the other challenges associated with non-vertical ensonification of marine organisms, such as the increased variability of target strength with fish orientation (Cutter and Demer, 2007), acoustic extinction (Foote et al., 1992; Zhao and Ona, 2003), and multiple scattering between single targets (Stanton, 1983).

We anticipate that the quantitative use of omni-directional sonars will increase in the near future, due to increased availability of sonars on fishery research vessels as well as an increasing use of sonar-equipped fishing vessels for fisheries surveys. The work presented here will facilitate the use of these sonars.

5. Summary

For the calibration and characterisation of omni-directional sonar performance we recommend the following activities:

1. Verify the range accuracy and apply a correction if necessary,
2. Measure the on-axis gain in adjacent beams. Repeat this for three well-separated directions,
3. Calibrate with sonar settings that are as close as possible to the survey settings, or derive relationships to compensate for differences between calibration and survey settings,
4. Measure the vertical and horizontal beamwidth to estimate the equivalent beam angle.

Acknowledgements

The authors acknowledge the valuable contributions of Atle Totland in helping to carry out and develop the calibration procedures and equipment. This work was funded by the Norwegian Research

Council through Grant Numbers 216460 (WHOFISH — Whale counting and fish school biomass appraisal by two new omni-directional fishery sonars) and 203477 (CRISP Centre for Research-based Innovation in Sustainable Fish Capture and Processing Technology). The cooperation and enthusiasm of the skippers and crew of *RV G.O. Sars*, *FV Artus*, *Brennholm*, *Eros*, and *Kings Bay* is gratefully acknowledged.

References

Ben-Yami, M., 1994. Purse Seining Manual. Fishing News Books, Oxford.
Bernasconi, M., 2012. The use of active sonar to study cetaceans ((Ph.D. thesis)), University of St Andrews.
Blomberg, A.E.A., Austeng, A., Hansen, R.E., 2012. Adaptive beamforming applied to a cylindrical sonar array using an interpolated array transformation. IEEE J. Ocean. Eng. 37, 25–34. http://dx.doi.org/10.1109/JOE.2011.2169611.
Brehmer, P., Gerlotto, F., 2001. A simple standardisation of omnidirectional sonar in fisheries research through field calibration and sampling data. Hydroacoustics 4, 27–30.
Brehmer, P., Lafont, T., Georgakarakos, S., Josse, E., Gerlotto, F., Collet, C., 2006. Omnidirectional multibeam sonar monitoring: applications in fisheries science. Fish Fish. 7, 165–179. http://dx.doi.org/10.1111/j.1467-2979.2006.00218.x.
Burdic, W.S., 1991. Underwater Acoustic System Analysis. Prentice Hall.
Chen, C.-T., Millero, F.J., 1977. Speed of sound in seawater at high pressures. J. Acoust. Soc. Am. 62, 1129–1135. http://dx.doi.org/10.1121/1.381646.
Cochrane, N.A., Li, Y., Melvin, G.D., 2003. Quantification of a multibeam sonar for fisheries assessment applications. J. Acoust. Soc. Am. 114, 745–758. http://dx.doi.org/10.1121/1.1587151.
Cutter, G.R., Demer, D.A., 2007. Accounting for scattering directivity and fish behaviour in multibeam-echosounder surveys. ICES J. Mar. Sci. 64, 1664–1674. http://dx.doi.org/10.1093/icesjms/fsm151.
Dalen, J., Løvik, A., 1981. The influence of wind–induced bubbles on echo integration surveys. J. Acoust. Soc. Am. 69, 1653–1659. http://dx.doi.org/10.1121/1.385943.
Demer, D.A., Berger, L., Bernasconi, M., Boswell, K.M., Chu, D., Domokos, R., Dunford, A.J., Fässler, S.M.M., Gauthier, S., Hufnagle, L.T., Jech, J.M., Bouffant, N., Lebourges-Dhaussy, A., Lurton, X., Macaulay, G.J., Perrot, Y., Ryan, T.E., Parker-Stetter, S., Stienessen, S., Weber, T.C., Williamson, N.J., 2015. Calibration of acoustic instruments, ICES Cooperative Research Report No. 326 No. 326, ICES.
Demer, D.A., Soule, M.A., Hewitt, R.P., 1999. A multiple–frequency method for potentially improving the accuracy and precision of in situ target strength measurements. J. Acoust. Soc. Am. 105, 2359–2376. http://dx.doi.org/10.1121/1.426841.
Fofonoff, P., Millard, R., 1983. Algorithms for computation of fundamental properties of seawater. UNESCO Tech. Pap. Mar. Sci. 44, 53.
Foote, K.G., Chu, D., Hammar, T.R., Baldwin, K.C., Mayer, L.A., Hufnagle Jr, L.C., Jech, M.J., 2005. Protocols for calibrating multibeam sonar. J. Acoust. Soc. Am. 117, 2013–2027. http://dx.doi.org/10.1121/1.1869073.
Foote, K.G., Knudsen, H.P., Vestnes, G., Maclennan, D.N., Simmonds, E.J., 1987. Calibration of acoustic instruments for fish density estimation: a practical guide. Int. Counc. Explor. Sea 69.
Foote, K.G., MacLennan, D.N., 1984. Comparison of copper and tungsten carbide calibration spheres. J. Acoust. Soc. Am. 75, 612–616. http://dx.doi.org/10.1121/1.390489.
Foote, K.G., Ona, E., Toresen, R., 1992. Determining the extinction cross section of aggregating fish. J. Acoust. Soc. Am. 91, 1983–1989. http://dx.doi.org/10.1121/1.403682.
Francois, R.E., Garrison, G.R., 1982. Sound absorption based on ocean measurements. Part II: Boric acid contribution and equation for total absorption. J. Acoust. Soc. Am. 72, 1879–1890. http://dx.doi.org/10.1121/1.388673.
Geoffroy, M., Rousseau, S., Knudsen, F.R., Fortier, L., 2015. Target strengths and echotraces of whales and seals in the Canadian Beaufort Sea. ICES J. Mar. Sci. fsv182, http://dx.doi.org/10.1093/icesjms/fsv182.
Hickling, R., 1962. Analysis of echoes from a solid elastic sphere in water. J. Acoust. Soc. Am. 34, 1582–1592. http://dx.doi.org/10.1121/1.1909055.
Holmin, A.J., Handegard, N.O., Korneliussen, R.J., Tjostheim, D., 2012. Simulations of multi-beam sonar echos from schooling individual fish in a quiet environment. J. Acoust. Soc. Am. 132, 3720–3734. http://dx.doi.org/10.1121/1.4763981.
Jech, J.M., Foote, K.G., Chu, D., Hufnagle Jr., L.C., 2005. Comparing two 38-kHz scientific echosounders. ICES J. Mar. Sci. 62, 1168–1179. http://dx.doi.org/10.1016/j.icesjms.2005.02.014.
Knudsen, H.P., 2009. Long-term evaluation of scientific-echosounder performance. ICES J. Mar. Sci. 66, 1335–1340. http://dx.doi.org/10.1093/icesjms/fsp025.
Lanzoni, J.C., Weber, T.C., 2011. A method for field calibration of a multibeam echo sounder, in: OCEANS 2011. Presented at the OCEANS 2011, pp. 1–7.
Lichte, H., 1919. Über den Einflußhorizontaler Temperaturschichtung des Seewassers auf die Reichweite von Unterwasser-schallsignalen (On the influence of horizontal temperature layers in sea water on the range of underwater sound signals). Phys. Z. 17, 385–389.
Lunde, P., Korneliussen, R.J., 2016. Power-budget equations and calibration factors for fish abundance estimation using scientific echo sounder and sonar systems. J. Mar. Sci. Eng. 4, 43. http://dx.doi.org/10.3390/jmse4030043.
MacLennan, D.N., 1981. The theory of solid spheres as sonar calibration targets (Scottish Fisheries Research Report Number 22). Department of Agriculture and Fisheries for Scotland.
MacLennan, D.N., Fernandes, P., Dalen, J., 2002. A consistent approach to definitions and symbols in fisheries acoustics. ICES J. Mar. Sci. 59, 365–369. http://dx.doi.org/10.1006/jmsc.2001.1158.
Medwin, H., Clay, C.S., 1998. Fundamentals of Acoustical Oceanography. Academic Press, Boston.
Melvin, G., Cochrane, N.A., Li, Y., 2003. Extraction and comparison of acoustic backscatter from a calibrated multi- and single-beam sonar. ICES J. Mar. Sci. 60, 669–677. http://dx.doi.org/10.1016/S1054-3139(03)00055-9.
Misund, O.A., 1990. Sonar observations of schooling herring: school dimensions, swimming behaviour, and avoidance of vessel and purse seine, in: Rapp. Procès-Verbaux La Réun. Cons. Perm. Int. Pour Explor. Mer 189, 135–146.

Misund, O.A., 1993. Abundance estimation of fish schools based on a relationship between school area and school biomass. Aquat. Living Resour. 6, 235–241. http://dx.doi.org/10.1051/alr:1993024.
Misund, O.A., Øvredal, J.T., Hafsteinsson, M.T., 1996. Reactions of herring schools to the sound field of a survey vessel. Aquat. Living Resour. 9, 5–11. http://dx.doi.org/10.1051/alr:1996002.
Nishimori, Y., Iida, K., Furusawa, M., Tang, Y., Tokuyama, K., Nagai, S., Nishiyama, Y., 2009. The development and evaluation of a three-dimensional, echo-integration method for estimating fish-school abundance. ICES J. Mar. Sci. 66, 1037–1042. http://dx.doi.org/10.1093/icesjms/fsp053.
Ona, E., Mazauric, V., Andersen, L.N., 2009. Calibration methods for two scientific multibeam systems. ICES J. Mar. Sci. J. Cons. 66, 1326–1334. http://dx.doi.org/10.1093/icesjms/fsp125.
Peraltilla, S., Bertrand, S., 2014. In situ measurements of the speed of Peruvian anchovy schools. Fish. Res. 149, 92–94. http://dx.doi.org/10.1016/j.fishres.2013.09.002.
Perrot, Y., Brehmer, P., Roudaut, G., Gerstoft, P., Josse, Erwan, 2014. Efficient multibeam sonar calibration and performance evaluation. Int. J. Eng. Sci. Innov. Technol. 3, 808–820.
Reynisson, P., 1998. Monitoring of equivalent beam angles of hull-mounted acoustic survey transducers in the period 1983–1995. ICES J. Mar. Sci. 55, 1125–1132. http://dx.doi.org/10.1006/jmsc.1998.0369.
Sherman, C.H., Butler, J.L., 2007. Transducers and arrays for underwater sound. In: Transducers and Arrays for Underwater Sound. Springer, http://dx.doi.org/10.1007/978-0-387-33139-3.
Simmonds, J., MacLennan, D., 2005. Fisheries Acoustics. Theory and Practice, second ed.. Blackwell Science, Oxford.
Skarthhamar, J., Svendsen, H., 2010. Short-term hydrographic variability in a stratified Arctic fjord. Geol. Soc. Lond. Spec. Publ. 344, 51–60. http://dx.doi.org/10.1144/SP344.5.
Smith, P.E., 1970. The horizontal dimensions and abundance of fish schools in the upper mixed layer as measured by sonar, in: Proceedings of an International Symposium on Biological Sound Scattering in the Ocean. Virginia, USA, pp. 563–599.
Stanton, T.K., 1983. Multiple scattering with applications to fish–echo processing. J. Acoust. Soc. Am. 73, 1164–1169. http://dx.doi.org/10.1121/1.389287.
Stockwell, J.D., Weber, T.C., Baukus, A.J., Jech, J.M., 2013. On the use of omnidirectional sonars and downwards-looking echosounders to assess pelagic fish distributions during and after midwater trawling. ICES J. Mar. Sci. J. Cons. 70, 196–203. http://dx.doi.org/10.1093/icesjms/fss139.
Tang, Y., Nishimori, Y., Furusawa, M., 2009. The average three-dimensional target strength of fish by spheroid model for sonar surveys. ICES J. Mar. Sci. 66, 1176–1183. http://dx.doi.org/10.1093/icesjms/fsp080.
Trygonis, V., Georgakarakos, S., Dagorn, L., Brehmer, P., 2016. Spatiotemporal distribution of fish schools around drifting fish aggregating devices. Fish. Res. 177, 39–49. http://dx.doi.org/10.1016/j.fishres.2016.01.013.
Trygonis, V., Georgakarakos, S., Simmonds, E.J., 2009. An operational system for automatic school identification on multibeam sonar echoes. ICES J. Mar. Sci. 66, 935–949. http://dx.doi.org/10.1093/icesjms/fsp135.
Vatnehol, S., Totland, A., Ona, E., 2015. Two mechanical rigs for field calibration of multi-beam fishery sonars. Methods Oceanogr. 13–14, 1–12. http://dx.doi.org/10.1016/j.mio.2016.02.001.
Zhao, X., Ona, E., 2003. Estimation and compensation models for the shadowing effect in dense fish aggregations. ICES J. Mar. Sci. 60, 155–163. http://dx.doi.org/10.1006/jmsc.2002.1319.